A COMPLEX MODE APPROACH FOR THE VALIDATION OF FE MODELS WITH STRUCTURAL DAMPING

Nicolas ROY (1), **Thomas LARROQUE** (2), **Tiana BRAULT** (3), **Fabrice BUFFE** (4)

(1) TOP MODAL, Ecoparc II, av. José Cabanis, 31130 Quint-Fonsegrives, FRANCE
Tel. +33 (0) 5 61 83 59 72 - e-mail nicolas.roy@topmodal.fr

(2) INGELIANCE Technologies, 6 rue Nicolas Leblanc, 33700 Mérignac, FRANCE
Tel. +33 (0) 5 57 92 41 70 - e-mail thomas.larroque@ingeliance.com

(3) HERAKLES - SAFRAN Group, Les Cinq Chemins, 33185 Le Haillan, FRANCE
Tel. +33 (0) 5 57 20 65 28 - e-mail tiana.brault@herakles.com

(4) CNES, 18, av. Edouard Belin, 31401 Toulouse Cedex 9, FRANCE
Tel. +33 (0) 5 61 28 34 65 - e-mail fabrice.buffe@cnes.fr

ABSTRACT

Dynamic analysis in the low and mid frequencies is generally performed using normal mode superposition techniques which offer numerical efficiency along with ease of physical interpretation.
The use of modal damping associated with the real modes is suitable for lightly damped structures with well separated modes. However, for structures with heavily damped materials or damping mechanisms the assumption of modal damping may no longer be valid.

To better account for the presence of damping in the structure, a complex mode approach based on structural damping is proposed as an effective alternative to the real mode approach.

1. INTRODUCTION

During the launch phase the mechanical environment is very severe - thus requiring extensive analysis of the dynamic behavior of launch vehicles and payloads. The associated FE models must be as accurate and predictive as possible.
Validation of FE models is often performed using a real mode approach by comparing the undamped (normal) modes of the FE model with those obtained through experimental modal analysis (EMA). In this case damping is represented by uncoupled modal damping factors under the assumption that the structure is lightly and evenly damped, and that the modes are well separated.

However, spacecraft and launch vehicles often contain sources of high local damping. Satellites are often designed with damping technologies as an effective way to achieve performance goals by reducing critical response levels. Solid Rocket Motors (SRM) have highly damped propellant which accounts for the majority of the total mass. This requires explicit modeling of the damping properties in the FE model - often in the form of structural (material) damping. In this case the underlying assumption of modal damping may no longer be valid.

To account for the presence of coupled damping in the structure, a complex mode approach based on structural damping is proposed as an effective alternative to the real mode approach.

In the first part of this paper the mode-superposition theory expressed in terms of the complex modes of a system with structural damping is presented. Since structural damping is associated with the (complex) stiffness matrix, there is no need to transform the system to a state-space ($2N$) model as in the case of viscous damping. As a consequence the resulting complex modes are much easier to interpret and implement. The notions involving orthogonality, modal effective parameters, modal energies and sensitivity analysis are presented and shown to be similar to their real mode counterparts.

Next, the identification of complex modes based on structural damping is presented. The RTMVI method originally formulated for real modes has been extended to complex modes using the same frequency domain least-squares fitting approach. Criteria for assessing the "degree of complexity" and for comparing complex modes are also presented.

Finally to illustrate the interest of model validation using complex modes, two industrial applications are presented involving a satellite structure and a SRM.

2. THEORY

2.1 Introduction

Structural or hysteretic damping based on the notion of a complex modulus is commonly used in the calculation of steady state responses. It can be easily modeled using loss factors associated with the different materials of the structure.

The main difference between structural and viscous damping is that the energy dissipated per cycle is proportional to the excitation frequency for viscous damping, whereas for structural damping it is independent of the frequency.

The principal limitation of structural damping is that it can be used only for frequency analysis due to the presence of a complex stiffness. Structural damping is therefore incompatible with transient and static analyses. In these cases structural damping can be approximated by equivalent viscous damping.

In the following, structural damping is assumed to be the only source of dissipation in the structure, and analysis is limited to frequency domain.

The reader may refer to [1] for further details on the theory presented hereafter.

2.2 Matrix Notation

A matrix is designated using a bold face character along with indices relating to its rows and columns (e.g. $\mathbf{X}_{ij}$). The transpose of a matrix is written by permuting its indices ($\mathbf{X}_{ij}{}^{T} = \mathbf{X}_{ji}$). Transposed complex matrices are *not* conjugated.

2.3 Complex Modes

In the frequency domain, the equations of motion for a discretized structure with structural damping can be written as

$$(-\omega^2\,\mathbf{M} + \mathbf{K} + i\,\mathbf{H})\,\mathbf{u}(\omega) = \mathbf{F}(\omega) \qquad (1)$$

where $\mathbf{H}$ is the structural damping matrix obtained by assembly of each element's stiffness matrix $\mathbf{K}_e$ and corresponding loss factor η_e according to the following expression.

$$\mathbf{H} = \sum_e \mathbf{K}_e\,\eta_e \qquad (2)$$

The equations of motion in Eq. (1) can be expressed using the complex stiffness $\hat{\mathbf{K}} = \mathbf{K} + i\,\mathbf{H}$ resulting in

$$(-\omega^2\,\mathbf{M} + \hat{\mathbf{K}})\,\mathbf{u}(\omega) = \mathbf{F}(\omega) \qquad (3)$$

It is important to note here that the complex stiffness matrix $\hat{\mathbf{K}}$ is symmetric (*not* Hermitian) since both $\mathbf{K}$ and $\mathbf{H}$ are symmetric.

Finally, partitioning Eq. (3) in terms of internal DOF, i and junction DOF, j leads to

$$\left(-\omega^2\begin{bmatrix}\mathbf{M}_{ii} & \mathbf{M}_{ij}\\ \mathbf{M}_{ji} & \mathbf{M}_{jj}\end{bmatrix} + \begin{bmatrix}\hat{\mathbf{K}}_{ii} & \hat{\mathbf{K}}_{ij}\\ \hat{\mathbf{K}}_{ji} & \hat{\mathbf{K}}_{jj}\end{bmatrix}\right)\begin{bmatrix}\mathbf{u}_i(\omega)\\ \mathbf{u}_j(\omega)\end{bmatrix} = \begin{bmatrix}\mathbf{F}_i(\omega)\\ \mathbf{F}_j(\omega)\end{bmatrix} \qquad (4)$$

The fixed-junction complex modes are obtained by directly solving the following eigenvalue problem.

$$(\hat{\mathbf{K}}_{ii} - \hat{\omega}_k^2\,\mathbf{M}_{ii})\,\mathbf{\Phi}_{ik} = \mathbf{0} \qquad (5)$$

Each mode k is represented by a complex eigenvalue $\hat{\omega}_k^2$ and an associated complex eigenvector $\mathbf{\Phi}_{ik}$.

This is in contrast with the use of viscous damping which requires rewriting the system to standard form in $2N$ space, and as a consequence produces N conjugate pairs of modes.

By comparison with the 1-DOF system, the undamped natural frequency ω_k and structural damping factor η_k can be obtained using the following relation

$$\hat{\omega}_k^2 = \omega_k^2\,(1 + i\,\eta_k) \qquad (6)$$

2.4 Orthogonality and Modal Energies

The complex modes will, in general, satisfy the same orthogonality conditions as for the normal modes, producing diagonal (uncoupled) matrices containing generalized masses $\mathbf{m}_k$ and generalized stiffnesses $\mathbf{k}_k$.

$$\mathbf{\Phi}_{ki}\,\mathbf{M}_{ii}\,\mathbf{\Phi}_{ik} = \mathbf{m}_k \qquad (7)$$

$$\mathbf{\Phi}_{ki}\,\mathbf{K}_{ii}\,\mathbf{\Phi}_{ik} = \mathbf{k}_k \qquad (8)$$

Note in the above equations that $\mathbf{\Phi}_{ki}$ designates the simple transpose of $\mathbf{\Phi}_{ik}$ and *not* its conjugate transpose!

The generalized masses and stiffnesses are complex values and related to the complex eigenvalue by the classical relation

$$\hat{\omega}_k^2 = \frac{k_k}{m_k} \qquad (9)$$

The modal energies are also complex valued and can be used in sensitivity analysis. Consider the derivative of the complex eigenvalue $\hat{\omega}_k^2$ with respect to a physical parameter x_p belonging to element *e* of the model. The well-known formula shown below can be applied directly using complex terms.

$$\frac{\partial \hat{\omega}_k^2}{\partial x_p} = \frac{\boldsymbol{\Phi}_{ki}(-\hat{\omega}_k^2 \frac{\partial \mathbf{M}_e}{\partial x_p} + \frac{\partial \hat{\mathbf{K}}_e}{\partial x_p})\boldsymbol{\Phi}_{ik}}{m_k} \tag{10}$$

Let's define the complex modal strain energy $U_k(e)$ for mode *k* and element *e* using the (real) element stiffness matrix $\mathbf{K}_e$ and complex modes as shown below.

$$U_k(e) = (\boldsymbol{\Phi}_{ke}\ \mathbf{K}_e\ \boldsymbol{\Phi}_{ek})/m_k \tag{11}$$

These energies can now be used in Eq. (10) to express the various sensitivities. For example, the derivative of the undamped eigenvalue with respect to the Young's modulus *E* of element *e* is given by

$$\frac{\partial \omega_k^2}{\partial E/E} = \Re U_k(e) - \eta_e\ \Im U_k(e) \tag{12}$$

The first term on the right-hand side is the same as in the real mode case whereas the second term arises from the use of complex modes.

Another example is the sensitivity of the undamped eigenvalue with respect to the loss factor η_e. The resulting expression shown below is strictly null when using real modes.

$$\frac{\partial \omega_k^2}{\partial \eta_e} = -\Im U_k(e) \tag{13}$$

A final interesting example is the sensitivity of the modal damping with respect to the loss factor given below. It can be used to evaluate the effectiveness of physical damping with respect to the modes.

$$\frac{\partial \eta_k}{\partial \eta_e} = \frac{1}{\omega_k^2}\left(\Re U_k(e) + \eta_k\ \Im U_k(e)\right) \tag{14}$$

2.5 Transformed Equations of Motion

The physical displacements $\mathbf{u}_i$ may be projected onto a basis comprising the complex modes $\boldsymbol{\Phi}_{ik}$ and static junction modes $\boldsymbol{\Psi}_{ij}$ according to the following linear transformation.

$$\begin{bmatrix} \mathbf{u}_i \\ \mathbf{u}_j \end{bmatrix} = \begin{bmatrix} \boldsymbol{\Phi}_{ik} & \boldsymbol{\Psi}_{ij} \\ \mathbf{0}_{jk} & \mathbf{I}_{jj} \end{bmatrix} \begin{bmatrix} \mathbf{q}_k \\ \mathbf{u}_j \end{bmatrix} \tag{15}$$

with

$$\boldsymbol{\Psi}_{ij} = -\hat{\mathbf{K}}_{ii}^{-1}\ \hat{\mathbf{K}}_{ij} \tag{16}$$

Note that the junction modes $\boldsymbol{\Psi}_{ij}$ are complex for a statically indeterminate (redundant) junction and real for a rigid junction.

Applying the transformation of Eq. (15) to Eq. (4) leads to the following uncoupled equations expressed in terms of the generalized displacements $\mathbf{q}_k$.

$$\left(-\omega^2 \begin{bmatrix} \mathbf{m}_k & \mathbf{L}_{kj} \\ \mathbf{L}_{jk} & \overline{\mathbf{M}}_{jj} \end{bmatrix} + \begin{bmatrix} \mathbf{k}_k & \mathbf{0} \\ \mathbf{0} & \overline{\mathbf{K}}_{jj} \end{bmatrix}\right) \begin{bmatrix} \mathbf{q}_k(\omega) \\ \mathbf{u}_j(\omega) \end{bmatrix} = \begin{bmatrix} \boldsymbol{\Phi}_{ki}\,\mathbf{F}_i(\omega) \\ \boldsymbol{\Psi}_{ji}\,\mathbf{F}_i(\omega) + \mathbf{F}_j(\omega) \end{bmatrix} \tag{17}$$

Note that this system has the same form as the undamped system with real modes. However, in the case of complex modes all the modal terms in Eq. (17) are complex-valued. For the special case of a rigid (statically determinate) junction, the condensed mass matrix $\overline{\mathbf{M}}_{jj}$ is real and the condensed stiffness matrix $\overline{\mathbf{K}}_{jj}$ is null.

2.6 Responses and Modal Effective Parameters

Solving Eq. (17) leads to the following FRF where $\mathbf{G}_{ii}(\omega)$ is the matrix of dynamic flexibilities, $\mathbf{T}_{ij}(\omega)$ the matrix of dynamic transmissibilities, and $\mathbf{M}_{jj}(\omega)$ the matrix of dynamic masses. Small terms, related to the junction mass, have been omitted from Eqs (20) and (21) for the sake of simplicity.

$$\begin{bmatrix} \mathbf{u}_i(\omega) \\ \mathbf{F}_j(\omega) \end{bmatrix} = \begin{bmatrix} \mathbf{G}_{ii}(\omega) & \mathbf{T}_{ij}(\omega) \\ -\mathbf{T}_{ji}(\omega) & -\omega^2 \mathbf{M}_{jj}(\omega) \end{bmatrix} \begin{bmatrix} \mathbf{F}_i(\omega) \\ \mathbf{u}_j(\omega) \end{bmatrix} \tag{18}$$

with

$$\mathbf{G}_{ii}(\omega) = \sum_{k=1}^{N} H_k(\omega)\ \tilde{\mathbf{G}}_{ii,k} \tag{19}$$

$$\mathbf{T}_{ij}(\omega) \approx \sum_{k=1}^{N} T_k(\omega)\ \tilde{\mathbf{T}}_{ij,k} \tag{20}$$

$$\mathbf{M}_{jj}(\omega) \approx \sum_{k=1}^{N} T_k(\omega)\ \tilde{\mathbf{M}}_{jj,k} \tag{21}$$

The contribution of a given mode, *k*, is expressed by the product of a dimensionless dynamic amplification,

$H_{\underline{k}}(\omega)$ or $T_{\underline{k}}(\omega)$, with the matrix of modal effective parameters ($\widetilde{\mathbf{G}}_{ii,k}$, $\widetilde{\mathbf{T}}_{ij,k}$, or $\widetilde{\mathbf{M}}_{jj,k}$) conveying the physical units and proper scaling to the response.

Note again that the form of Eqs. (19) - (21) is identical to that for the real mode approach. However the modal effective parameters are complex-valued.

2.7 Modal Identification

The RTMVI modal identification method [2-3] uses a least-squares curve-fitting technique to determine the three modal quantities - natural frequency, modal damping and modal effective parameter - based on the following general form of the FRF

$$X(\omega) = \sum_k A_k(\omega, \omega_k, \eta_k)\, \widetilde{X}_k \qquad (22)$$

where X designates the type of FRF (G, T or M), $A_k(\omega)$ the dynamic amplification ($H_k(\omega)$ or $T_k(\omega)$) and $\widetilde{X}_k$ the corresponding modal effective parameter.

In the case of real modes, the modal effective parameter $\widetilde{X}_k$ is assumed to be real-valued. Only the imaginary part of Eq. (22) is used in the curve-fitting process since it contains a simple resonant peak as opposed to the real part which has a more complicated shape as illustrated in Fig. 1. Moreover the real part is much more sensitive to the influence of neighboring modes.

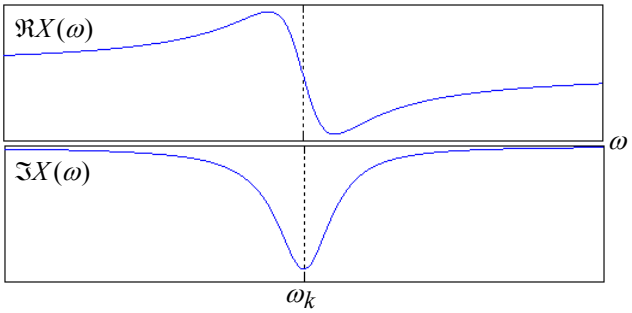

Figure 1: FRF Resonance using a Real Mode

To account for complex modes in the RTMVI method, the modal effective parameter of Eq. (22) is assumed complex. Four modal parameters must now be determined instead of three due to the addition of the imaginary part of $\widetilde{X}_k$.

Another complication arises from the fact that the complex-valued modal effective parameter introduces a change of phase in the response, and therefore the response at resonance is no longer in quadrature with the excitation. This means that the resonant peak is no longer associated with the imaginary part of the response as illustrated in Fig. 2.

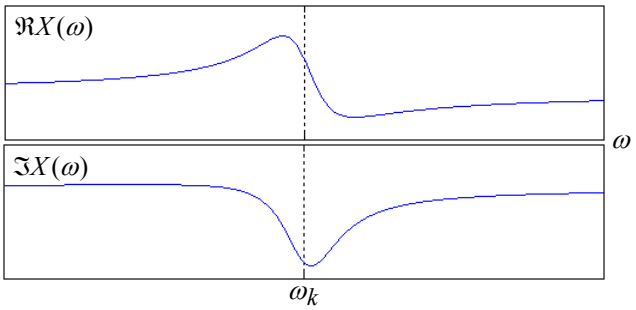

Figure 2: FRF Resonance using a Complex Mode

To account for the phase changes induced by the complex modes, the RTMVI method was modified to allow for curve-fitting using the real and/or imaginary parts of Eq. (22).

2.8 Complexity Criterion

A simple complexity criterion is proposed here to quantity the degree of complexity of any given mode shape. The criterion is based on the Modal Phase Collinearity (MPC) [4] and described hereafter.

Consider the complex mode shape $\mathbf{\Phi}_{ik}$ for mode k depicted in Fig. 3 with components plotted as points in the complex plane. The degree of linearity (correlation) of the points can be used as a measure of complexity.

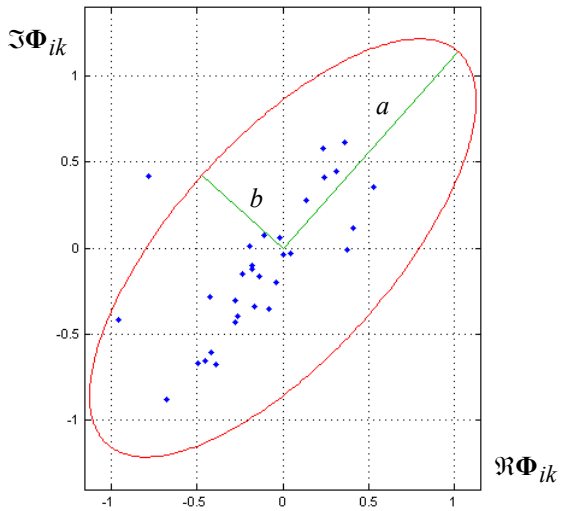

Figure 3: Complex Mode and Associated Ellipse

This is done by considering the 2x2 product matrix $\mathbf{B}_{kk}$ using the real and imaginary parts of $\mathbf{\Phi}_{ik}$.

$$\mathbf{B}_{kk} = \begin{bmatrix} \Re(\mathbf{\Phi}_{ki})\,\Re(\mathbf{\Phi}_{ik}) & \Re(\mathbf{\Phi}_{ki})\,\Im(\mathbf{\Phi}_{ik}) \\ \Re(\mathbf{\Phi}_{ki})\,\Im(\mathbf{\Phi}_{ik}) & \Im(\mathbf{\Phi}_{ki})\,\Im(\mathbf{\Phi}_{ik}) \end{bmatrix} \qquad (23)$$

From $\mathbf{B}_{kk}$ an ellipse can be constructed whose orientation is obtained from the eigenvectors of $\mathbf{B}_{kk}$, and whose semi-major and semi-minor axes *a* and *b* are obtained from the square root of the eigenvalues.

The complexity criterion c_k is defined simply as the ratio of the semi-minor axis to the semi-major axis.

$$c_k = \frac{b}{a} \quad \text{with} \quad 0 \le c_k \le 1 \tag{24}$$

The value $c_k = 0$ indicates a real mode - in other words a mode shape with perfectly correlated real and imaginary parts. In this case the ellipse collapses to a line. The value $c_k = 1$ indicates a complex mode with uncorrelated real and imaginary parts in which case the ellipse becomes a circle.

2.9 Modal Assurance Criterion (MAC)

The modal assurance criterion or MAC [5-6] is used to compare and match mode shapes and can be readily extended to take into account complex modes resulting from structural damping.

In the case of viscous damping, the modes occur in conjugate pairs, requiring adaptations to the MAC [7]. This is not necessary in the present context.

The MAC can be derived by considering the distance *d* between two mode shapes *X* and *Y*

$$d = \left\| X - \beta Y \right\| \tag{25}$$

where the modal scale factor, β, takes into account the differences in amplitude and phase between *X* and *Y* in order to have two comparable vectors.

The optimal value for β which minimizes *d* for a given pair of mode shapes is given below where Y^* in this particular case designates the conjugate transpose of *Y*.

$$\beta = \frac{Y^* X}{Y^* Y} \tag{26}$$

The MAC is based on the distance, *d*, but bounded between 0 and 1, with 1 indicating identical mode shapes ($X = \beta Y$). This leads to the following expression.

$$MAC(X,Y) = 1 - \frac{d^2}{\left\| X \right\|^2} \quad [0,1] \tag{27}$$

Eq. (27) can be rewritten in the usual form:

$$MAC(X,Y) = \frac{\left\| X^* Y \right\|^2}{\left\| X \right\|^2 \left\| Y \right\|^2} \quad [0,1] \tag{28}$$

The above expression can be used with both real and complex modes.

3. INDUSTRIAL APPLICATIONS

3.1 Satellite Structure

Microscope is a microsatellite of the CNES Myriade series dedicated to fundamental physics. The main objective of the satellite is to verify the Equivalence Principle with an extremely high accuracy.

The finite element model of the payload assembly is shown in Fig. 4 and constitutes the structure that houses the two accelerometers used to measure and compare the free fall velocities of two test masses.

The model comprises approximately 25 000 nodes. The upper part of the payload structure is isolated from the lower via damped springs (PBUSH entries) with a loss factor of $\eta = 0.34$. No other damping was introduced in the model.

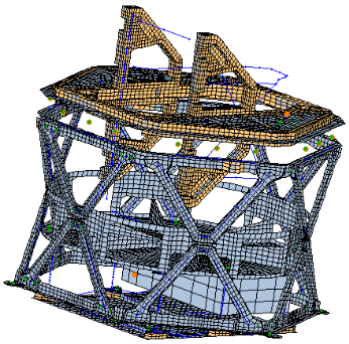

Figure 4: FE Model of Microscope Payload

Both normal mode analysis (SOL 103) and complex mode analysis (SOL 107) was performed using MSC/NASTRAN with the Lanczos method.

The computation time for extracting 25 modes was 43 seconds for the real modes and 100 seconds for the complex modes. A comparison of the first 20 modes is presented in Fig. 5.

Mode No.	Normal (Hz)	Complex (Hz)	Freq. (% Err)	MAC
1	81.144	82.077	-1.14	0.99
2	86.690	87.529	-0.96	1.00
3	93.537	94.585	-1.11	1.00
4	103.994	105.153	-1.10	0.99
5	127.429	129.042	-1.25	1.00
6	185.536	185.540	-0.00	1.00
7	188.707	191.122	-1.26	0.97
8	210.382	210.467	-0.04	1.00
9	216.457	216.460	-0.00	0.99
10	241.833	241.865	-0.01	1.00
11	283.098	283.101	-0.00	1.00
12	308.056	312.055	-1.28	0.65
13	312.907	313.853	-0.30	0.74
14	346.338	349.564	-0.92	0.74
15	356.002	355.173	0.23	0.62
16	379.501	382.165	-0.70	0.95
17	388.700	388.616	0.02	0.98
18	401.505	401.700	-0.05	1.00
19	433.459	436.158	-0.62	0.82
20	435.289	437.703	-0.55	0.76

Figure 5: Real vs. Complex Modes

Note that the natural frequencies associated with the complex modes are overall greater (up to ~1%) than the frequencies of the normal modes. As for the mode shapes, the MAC values remain high for the lower modes and degrade in the vicinity of close modes.

The differences could lead to improved model validation when comparing with the experimentally derived complex modes using RTMVI.

3.2 Solid Rocket Motor

The dynamic behavior of solid rocket motors (SRM) plays an important role in their development. Frequency specifications must be strictly respected to avoid dynamic amplification within the SRM and coupling with the payload.

To verify conformity with the specifications, dynamic testing is performed in order to identify the modes of the SRM and to qualify the SRM with respect to the dynamic environment. This involves single-axis base excitation vibration tests using sine, random or shock excitation. The SRM test setup and FE model are illustrated in Fig. 6.

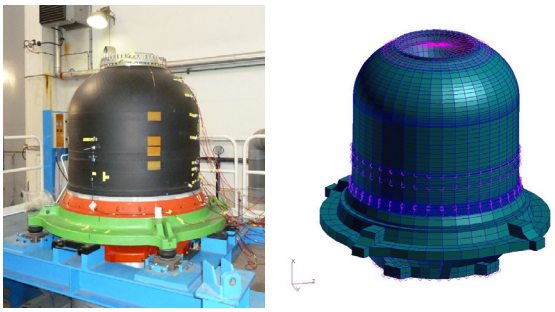

Figure 6: Vibration Test Setup and FE Model

The results presented here come from a longitudinal sine-sweep qualification test. Using the measured FRF, real modes were identified using RTMVI and compared to the real modes obtained from FE modal analysis.

The modal correlation was overall satisfactory (frequency errors < 10% and MAC values greater than 0.8), however certain discrepancies were observed between the test FRF and the synthesized FRF using the identified real modes as shown in Fig. 7. These errors were reduced when identifying with complex modes.

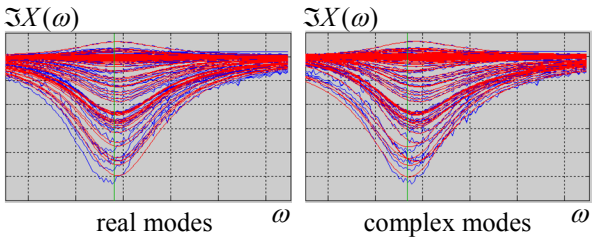

Figure 7: FRF Synthesis - Low Frequency Mode

At a higher frequency an observed resonance in the test FRF was never able to be identified using normal modes. With complex modes, the peak was easily identifiable and the resulting synthesis was very good as shown in Fig. 8. The complexity criterion for this mode was relatively high (~25 %).

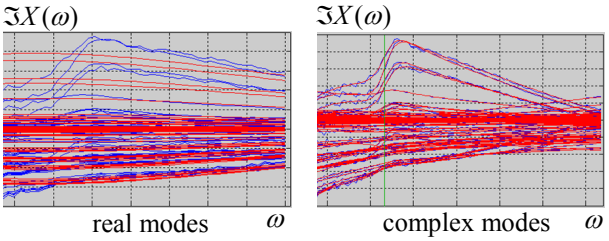

Figure 8: FRF Synthesis - High Frequency Mode

4. CONCLUSIONS

A complex mode approach based on structural damping has been proposed as an alternative to the classical normal mode approach for response analysis, modal identification and model validation in the frequency domain.

The mode-superposition theory adapted to the complex modes of a system with structural damping has been presented. The concepts of orthogonality, modal effective parameters, modal energies and sensitivity analysis require certain adaptations but remain similar to their real mode counterparts.

The RTMVI modal identification method has been extended to complex modes by the use of complex-valued modal effective parameters. Therefore the same modal parameters (frequency, damping and modal effective parameter) are used for identifying normal or complex modes.

Preliminary results involving the use of complex modes in industry are promising. The presence of highly damped materials and damping mechanisms in today's structures should encourage the use of complex modes in the future.

5. REFERENCES

[1] Girard A., Roy N., *Structural Dynamics in Industry,* ISTE Ltd and John Wiley & Sons, ISBN 978-1-84821-004-2, 2008.

[2] Girard A., Roy N., Guyot M., Bugeat L.-P., *Modal Identification via Effective Parameters: An Industrial Solution*, European Conference on Spacecraft Structures, Materials and Mechanical Testing, Proceedings ESA SP-468, p. 283-288, March 2001.

[3] Lefevre Y.M., Bonetti J.C., Girard A., Roy N., Calvi A., *Real Time Modal Identification Techniques for Improved Satellite Vibration Testing*, Proceedings, European Conference on Spacecraft Structures, Materials and Mechanical Testing, Toulouse, France, Dec. 2002.

[4] Pappa R. S., Elliott K. B., Schenk A., *Consistent-mode Indicator for the Eigensystem Realization Algorithm*, Journal of Guidance, Control and Dynamics, 16(5), pp. 852-858, September-October 1993.

[5] Allemang R. J., Brown D. L., *A Correlation Coefficient for Modal Vector Analysis*, Proceedings, International Modal Analysis Conference, pp. 110-116, 1982.

[6] Allemang R. J., *The Modal Assurance Criterion: Twenty Years of Use and Abuse*, Sound and Vibration Magazine, 37(8), pp. 14-23, 2003.

[7] Vacher P., Jacquier B., Bucharles A., *Extensions of the MAC Criterion to Complex Modes*, Proceedings, ISMA, 2010.